Crystal Morphogenesis

Deutsche Ausgabe: DOI: 10.1002/ange.201607221
Internationale Ausgabe: DOI: 10.1002/anie.201607221

Poly(ionic liquid)-Mediated Morphogenesis of Bismuth Sulfide with a Tunable Band Gap and Enhanced Electrocatalytic Properties

Min-Rui Gao, Shu-Hong Yu, Jiayin Yuan, Weiyi Zhang, and Markus Antonietti**

Abstract: *Conventional polymer additives have a substantial impact on synthetic inorganic chemistry, but critical shortcomings remain; for example, low solubility in organic solvents and potential thermodynamic aggregates. Poly(ionic liquid)s have now been used as efficient additives that enable a high level control of bismuth sulfide crystals with significant size and morphological diversities. The bismuth sulfides exhibit tunable band structure as a result of the quantum size effects. Moreover, poly(ionic liquid)s are able to couple with as-synthesized bismuth sulfides chemically and endow a modified surface electronic structure, which allows resultant products to possess outstanding electrocatalytic performance for water oxidation, although its commercial counterpart is catalytically inert.*

The creation of inorganic materials with tailored structures and morphologies has continued advancing materials chemistry by offering new properties and applications.[1] Previous synthesis using polymers as stabilizers and crystal growth modifiers has achieved substantial success in making systems with targeted properties.[2] For instance, double hydrophilic block copolymers have proven to be efficient additives for accessing inorganic micro-/nanoobjects with controlled morphologies and superstructures, where the single functional blocks can modulate specific polymer–crystal interactions.[2] However, shortcomings, such as low solubility in organic solvents and potential thermodynamic aggregates,[3] place limits on the use of these polymers. Recently, a new family of polymers, namely poly(ionic liquid)s (PILs), was obtained from ionic liquid monomers,[4] which combine the unique features of ionic liquids, including high ionic conductivity, high thermal and chemical stabilities,[4a,b] together with polymer properties, such as multivalency, multifunctionality, intrinsic dimensions, and ease of processing.[4,5] These merits, coupling with their good solubility in organic solvents, suggested that the use of PILs as additives in inorganic synthesis might lead to methods of creating newly structured materials, which, however, has remained unexplored.

We wanted to illustrate this prospect by applying PILs as additives for the morphogenesis of transition-metal chalcogenides, because they are fundamentally and technologically attractive for a variety of applications.[1a,6] As a highly photoconductive semiconductor, bismuth sulfide (Bi_2S_3) has a direct band gap (E_g) of about 1.3 eV, approaching to the idea value (1.34 eV) for maximum photovoltaic efficiency.[7] This material was also described to substantially impact across diverse research fields such as thermoelectric cooling,[8] gas sensing,[9] biomolecule detection,[10] thermoradiotherapy,[11] and X-ray computed tomography imaging.[12] Bi_2S_3 often crystallizes in a layered structure that leads to strong anisotropy in electronic and lattice properties.[13] Present approaches for making Bi_2S_3 described overwhelmingly one-dimensional (1D) structures,[10,14] because of its highly anisotropic crystal structure consisting of infinite chains of covalently bound atoms.[15] This is on the one hand very attractive, but also limits the further development of Bi_2S_3, particularly regarding the integration of the nanoscale materials in devices, where the electronic and semiconductor properties are known to be morphology- and size-dependent.[7b,14a,16] Therefore, effective strategies that enable the morphogenesis of Bi_2S_3 with unique structures, high-pure phase, and good crystallinity are appealing both scientifically and technologically for applications.

Herein, we report the first use of PILs as effective additives to modify the nucleation and growth of Bi_2S_3 materials from organic solvents, which leads to unique crystals with highly tailored sizes, dimensions, and architectures, and in consequence a tunable E_g owing to the quantum-size effect. A broad set of characterization techniques confirms that the participation of PILs can not only control the synthesis but also enable surface electronic structure modulation, endowing the resultant Bi_2S_3 to show highly enhanced electrocatalytic performance. This was illustrated by an important but difficult reaction, that is, the anodic water oxidation reaction of water electrolyzers, where it can compete with the reference RuO_2 catalyst, while its commercial counterpart is almost catalytically inactive. It is assumed that PIL additives can be generalized to the morphogenesis of a wide range of other functional materials, giving access to a broader tuning of new functionalities and properties.

We selected commercially available or readily synthesized PILs, including poly(1-methyl-3-(4-vinylbenzyl)-imidazolium chloride) (PIL-**1**), poly(diallyldimethylammonium bis(trifuoromethanesulfonyl)imide) (PIL-**2**), and poly(3-ethyl-1-vinylimidazolium bromide) (PIL-**3**), as additives for experiments, which all show exceptional solubility in *N*,*N*-dimethyl-

[*] Prof. Dr. M. R. Gao, Dr. J. Y. Yuan, W. Y. Zhang, Prof. Dr. M. Antonietti
Max Planck Institute for Colloids and Interfaces, Potsdam-Golm Science Park
Am Mühlenberg 1, 144776 Potsdam (Germany)
E-mail: markus.antonietti@mpikg.mpg.de
Prof. Dr. M. R. Gao, Prof. Dr. S. H. Yu
Division of Nanomaterials & Chemistry, Hefei National Laboratory for Physical Sciences at Microscale, Department of Chemistry, University of Science and Technology of China
Hefei 230026 (China)
E-mail: mgao@ustc.edu.cn

Supporting information for this article can be found under: http://dx.doi.org/10.1002/anie.201607221.

formamide (DMF), a polar organic solvent that is commonly used for conducting the synthesis of transition-metal chalcogenides.[6a,17] The syntheses were performed in a simple solvothermal system, composing of mixtures of DMF, $Bi(NO_3)_3$, CH_4N_2S, and PILs in appropriate ratios, which were then heated at desired temperature to induce crystallization (Figure 1; see also the Supporting Information for experimental details). Notably, the almost same synthesis with the three PIL additives resulted in a significant morphological diversity of the achieved materials, owing to their different cations, anions, and backbone architectures that selectively couple with specific crystal faces, to modulate and even template consecutive growth, strongly evidencing the effective role of PILs in modifying the crystal growth pattern (Figure 1). X-ray diffraction (XRD) patterns in Figure 2a support the formation of a pure orthorhombic Bi_2S_3 phase (JCPDS 170320), while lack of the PIL additive caused impurities in the final product (Supporting Information, Figure S1), suggesting the capability of PILs to suppress other crystallization events.

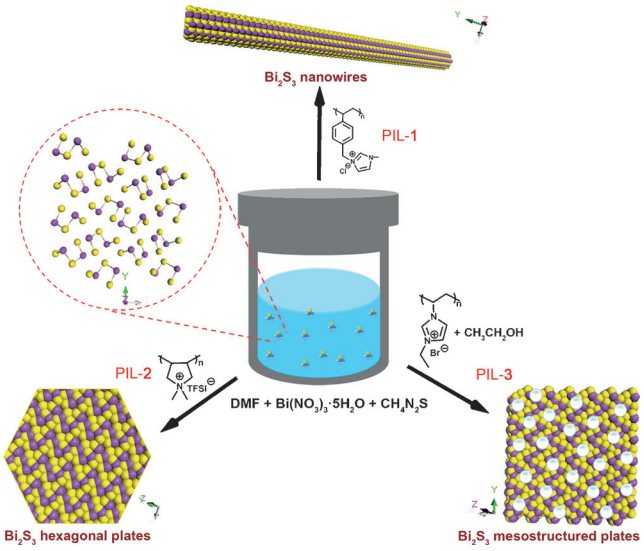

Figure 1. High-quality Bi_2S_3 crystals with significant morphological diversity are created by using various PILs as synthetic additives. Inset in the red dotted circle shows the crystal structure of Bi_2S_3 projected onto the (001) plane. Purple and yellow spheres indicate Bi and S atoms, respectively.

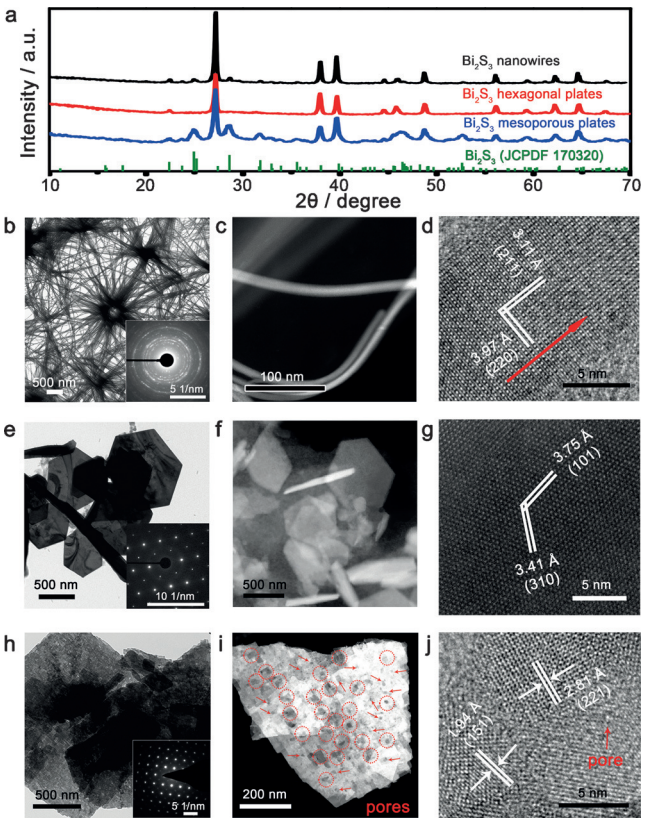

Figure 2. a) XRD patterns of as-prepared Bi_2S_3 nanowires, Bi_2S_3 hexagonal plates, and Bi_2S_3 mesoporous sheets. b) TEM, c) HAADF-STEM, and d) HRTEM images for Bi_2S_3 nanowires. Inset in panel (b) shows the corresponding SAED pattern. e) TEM, f) HAADF-STEM, and g) HRTEM images for Bi_2S_3 hexagonal plates. Inset in panel (e) shows the SAED pattern taken on a typical plate. h) TEM, i) HAADF-STEM, and j) HRTEM images for Bi_2S_3 mesoporous sheets. Inset in panel (h) shows the SAED pattern taken on a typical mesoporous sheet.

We used various characterization techniques to identify the morphology, crystal structure, and chemical composition of as-prepared Bi_2S_3 crystals (Figure 2b–j, Supporting Information, Figures S2–S7). Transmission electron microscopy (TEM) image of Bi_2S_3 controlled by PIL-**1** (Figure 2b) reveals the presence of three-dimensional networks composed of ultralong Bi_2S_3 nanowires (up to tens of micrometers). Corresponding selected-area electron diffraction (SAED) pattern shows polycrystalline features owing to the nanowires-constructed microstructure (Figure 2b, inset). High-angle annular dark-field scanning TEM (HAADF-STEM) image in Figure 2c shows that the nanowires are flexible, smooth and thin with diameter of about 12 nm. A high-resolution TEM (HRTEM) image demonstrates the high crystallinity of our Bi_2S_3 nanowires with resolved lattice fringes of (211) and (220) planes, indicating that they grow along the [110] direction (Figure 2d). Similar to some previously reported 1D Bi_2S_3 nanostructures,[14a,b] this growth direction deviates from the *c* axis. STEM elemental mapping shows a uniform spatial distribution of Bi and S (Supporting Information, Figure S2d). Furthermore, energy-dispersive X-ray (EDX) spectroscopy reveals the presence of N and Cl coming from PIL-**1** (Supporting Information, Figure S2c), indicating its participation in modifying the Bi_2S_3 growth. Intriguingly, these Bi_2S_3 nanowires readily form free-standing membranes as well as very thin film on appropriate substrates, such as glass (Supporting Information, Figure S3).

When the PIL-**1** used in the Bi_2S_3 nanowire synthesis was replaced by PIL-**2**, hexagonal Bi_2S_3 plates with edge lengths ranging from 500 nm to1 μm were achieved (Figure 2e and f). The SAED pattern of a typical Bi_2S_3 plate exhibits sixfold symmetry and single-crystalline character (Figure 2e, inset). No defects or disorders are observed on the high-crystalline Bi_2S_3 plates (Figure 2g), demonstrating the generation of very high-quality crystals. STEM elemental mapping confirms the

presence of Bi and S with uniform spatial distribution (Supporting Information, Figure S4a), while the N and F signals detected by EDX again reflect the presence of the PIL-**2** additive (Supporting Information, Figure S4b). As mentioned above, the growth of Bi_2S_3 is highly 1D anisotropic owing to its intrinsic crystal lattice symmetry.[15] The formation of the new 2D Bi_2S_3 structure therefore indicates strong structural control enabled by the PIL-**2**, which can regulate the growth rate of different crystallographic faces via selective adsorption,[2] leading to the inhibition of 1D growth, as confirmed by the observation of PIL-**2** binding on the achieved products (Supporting Information, Figure S5).

Interestingly, when the additive was switched to PIL-**3**, very unusual mesoporous Bi_2S_3 sheets were formed, here in the mixture solvent of DMF and ethanol, with lateral sizes of up to 2 μm (Figure 2h). Close-up inspection of these crystals shows that they are actually an assembled superstructure of tiny Bi_2S_3 flakes (Figure 2i, Supporting Information, Figure S6) with a mesopore size distribution between 2 to 4 nm and Brunauer–Emmett–Teller (BET) surface area of 68 $m^2 g^{-1}$ (Supporting Information, Figure S7). HRTEM image clearly confirms the presence of mesopores between highly crystalline Bi_2S_3 nanocrystals (Figure 2j). SAED taken from a large area of a Bi_2S_3 sheet produces single-crystal diffraction pattern (Figure 2h, inset), indicating the long-range vectorial alignment of the crystalline flakes, which leads to a new mesoporous single crystal,[2d] and it is, to the best of our knowledge, the first such example for Bi_2S_3. In contrast, in the absence of PIL additives, the exact same synthesis produced microsized aggregates with impure Bi_2S_3 phase (Supporting Information, Figure S1). Taken together with studies described above, our results highlight the efficient role of PILs in mediating the nucleation and growth of inorganic materials in a size and shape specific fashion, that is, morphosynthesis.

It is well-documented that bulk Bi_2S_3 displays an E_g of about 1.3 eV and it has been intensively explored as a photovoltaic material.[7] However, for some applications such as photocatalytic water splitting, this narrow E_g is not sufficiently large to drive the uphill reactions with theoretical energy requirements > 1.23 eV plus the known overpotentials (Supporting Information, Figure S8). Our PILs-controlled Bi_2S_3 crystals show a striking increase of the E_g (Figure 3), presumably due to the quantum size effects arising from a reduction of the crystal size.[18] An ultraviolet–visible (UV/Vis) spectrum (Figure 3) reveals that the Bi_2S_3 nanowires show an intrinsic semiconductor-like absorption in the red region of the visible spectrum with an E_g of 1.95 eV (Supporting Information, Figure S9). The E_g values of 2D Bi_2S_3 mesocrystalline sheets and hexagonal plates are estimated to be 1.73 and 1.54 eV, respectively, where the primary, nanoscale flake-like assembly units of the mesoporous sheets lead to more profound quantum size effects and thus larger E_g value (Figure 3; Supporting Information, Figure S9). It is noteworthy that PILs themselves do not contribute to the observed E_g tunability (Supporting Information, Figure S10). Photographs of the three as-made Bi_2S_3 crystals dispersed in ethanol display varied colors (Figure 3, inset). Of note, the Bi_2S_3 nanowires and hexagonal plates can form very stable

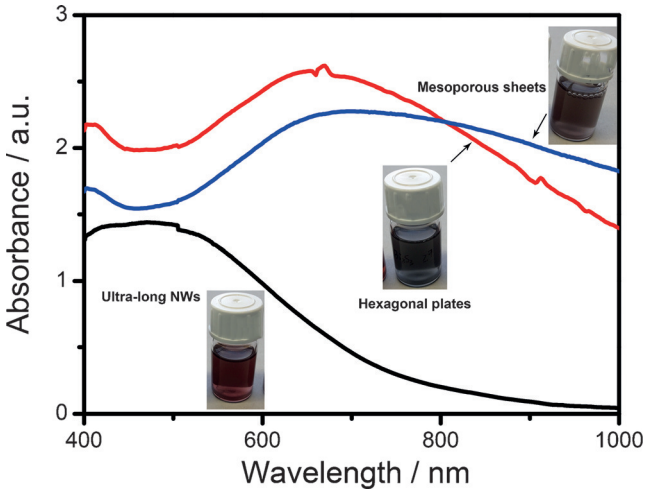

Figure 3. UV/Vis diffuse reflectance spectra of the as-prepared Bi_2S_3 crystals. Insets: photographs of corresponding Bi_2S_3 crystals dispersed in ethanol.

dispersions in ethanol, because of the electronic/steric protection resulting from residual PILs on crystal surfaces[19] (Supporting Information, Figure S11), while Bi_2S_3 mesoporous sheets in ethanol cause sediment, owing to only little PILs maintained after synthesis, which will be discussed beneath.

Fourier-transform infrared (FTIR) spectra (Supporting Information, Figure S12) further confirm the formation of the Bi_2S_3 phase, and moreover, show that certain PIL-**1** and PIL-**2** were retained after synthesis, in agreement with EDX and HRTEM results (Supporting Information, Figure S2c, Figure S4b, Figure S5a,b). However, when PIL-**3** was used, the synthesis led to Bi_2S_3 mesostructures with very little additives left on the surface (Supporting Information, Figure S12c), which is because that the usage of PIL-**3** was significantly smaller as compared to those of PIL-**1** and PIL-**2** (see Methods in the Supporting Information). Early reports have demonstrated that polymer additives left at the surface, if with an appropriate amount, can bring beneficial structural and electronic regulations, offering modified crystal facets, defect sites, or charged surfaces that enable promoted properties.[20] Such a promotional effect is supposed to be remarkably profound on PILs-modified materials, considering the presence of charged groups (cation and anion)[4a,c] that could allow for superior charge-structure modulation.[21]

We thus examined the change of surface chemical bonding of our prepared Bi_2S_3 crystals, with commercial Bi_2S_3 (Supporting Information, Figure S13) for comparison, by means of X-ray photoelectron spectroscopy (XPS) (Figure 4; Supporting Information, Figure S14 and S15). The binding energy of the S 2s electrons decreases by about 0.6 eV (referenced to the C 1s peak at 284.5 eV) for the three PILs-controlled samples relative to that of commercial Bi_2S_3 (Figure 4, left). In the Bi region (Figure 4, right), two sets of peaks corresponding to $4d_{5/2}$ (441.9 eV) and $4d_{3/2}$ (465.5 eV) core levels are observed for commercial Bi_2S_3, agreeing perfectly with previously reported results.[22] The Bi 4d signals shift towards higher energies, with increases by approximately 0.95, 0.41,

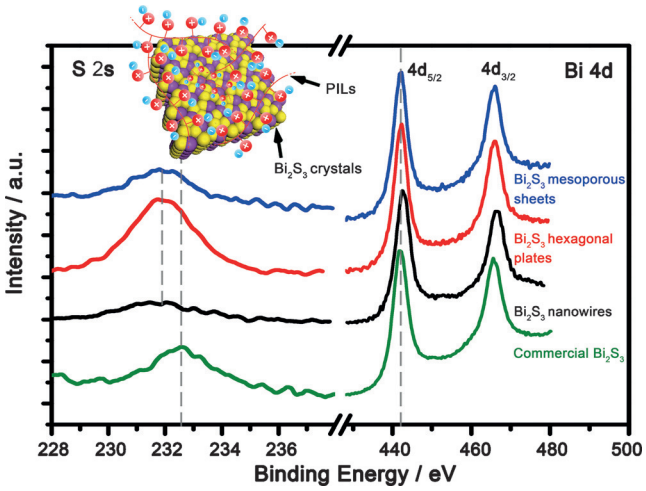

Figure 4. High-resolution XPS spectra of the S 2s (left) and Bi 4d (right) for the three as-prepared Bi_2S_3 crystals with the commercial counterpart as reference. Inset: structural model of the Bi_2S_3 surface modified with PILs.

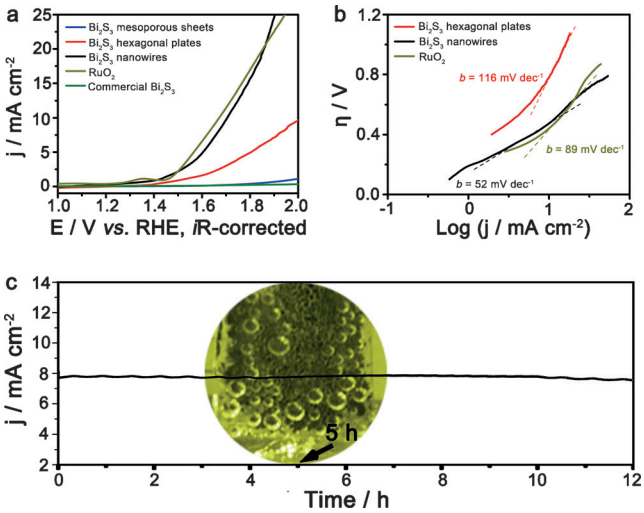

Figure 5. a) Polarization curves for OER on modified FTO electrodes comprising Bi_2S_3 crystals controlled from different PIL additives. Catalyst loading is approximate 0.28 mg cm^{-2} for all samples. Sweep rate: 10 mV s^{-1}. b) Tafel plots for various catalysts derived from (a). c) Chronoamperometric response (*j*–*t*) recorded from the as-prepared Bi_2S_3 nanowires at a constant overpotential of 400 mV. Inset: photograph showing O_2 bubbles accumulated on the Bi_2S_3-modified FTO electrode at the time point of 5 h. All the measurements were performed in N_2-saturated 0.1 M KOH (pH ≈ 13).

and 0.19 eV at $4d_{5/2}$ for PIL-**1**, PIL-**2**, and PIL-**3** modified Bi_2S_3, respectively (Supporting Information, Figure S14). Previous experimental and computational studies showed that charge transfer can occur from Bi to S and leads to increased energy on Bi and decreased energy on S, respectively, owing to the ionic feature of Bi_2S_3 crystal.[13] In the case of PILs-modified Bi_2S_3, the energy gains on the Bi vary significantly, while S shows constant energy loss, which suggests that PILs coupled to the Bi_2S_3 surface supports higher polarization of the Bi–S bond, leading to different chemical/electronic environments and hence potentially different catalytic properties. The observation of N 1s signals, which originate from PILs used only, provides evidence in support of such polymer driven coupling effects, whereas on commercial Bi_2S_3 no this signal was detected (Supporting Information, Figure S15).

One of emerging interests on Bi_2S_3 materials aims for exploring its photoelectrochemical catalytic capability,[23] but its conjunction with a co-catalyst is commonly needed to trap the photo-driven holes/electrons and consequently catalyze the desired reactions. Developing photoactive materials those are catalytically active themselves will simplify the electrode design and improve the conversion efficiency.[24] We therefore evaluated the ability of our crystalline Bi_2S_3 for catalyzing the oxygen-evolving reaction (OER), the anodic-half reaction of water electrolyzers, exploring a potential usefulness of their diverse structures and modified electronic features. Figure 5 a compares the current densities achieved within a anodic potential window onto fluorine-doped tin oxide (FTO) electrodes modified with various catalysts in 0.1 M KOH. The featureless polarization curve for commercial Bi_2S_3 demonstrates that it is OER inactive. Scanning anodically shows that the onset potential of OER occurs at approximately 1.46 V versus reversible hydrogen electrode (RHE) for the PIL-**1** modified Bi_2S_3 nanowires, even approaching the performance of a benchmark RuO_2 catalyst. In contrast, Bi_2S_3 hexagonal plates mediate OER at larger overpotential (η) of 1.58 V, while Bi_2S_3 mesoporous sheets provide negligible OER activity. Figure 5 b shows that a Tafel slope of 52 mV per decade was measured for the Bi_2S_3 nanowires, which is much smaller than that of Bi_2S_3 hexagonal plates, and unexpectedly, even smaller than that of RuO_2, indicating the efficient kinetics of O_2 evolution catalyzed by PIL-**1** modified Bi_2S_3 nanowires. Notably, the possibility of an OER enhancement by PILs as such can be excluded, because they only affect little OER activity (Supporting Information, Figure S16). We thus attribute this superior activity of the Bi_2S_3 nanowires to an electrocatalytic synergistic effect[25] between PIL-**1** and Bi_2S_3, which leads to modified surface electronic structure and a formal higher Bi oxidation state, improving the catalytically active sites on Bi_2S_3 for optimum O-intermediate adsorption.[26] Figure 5 c and inset reveal that the Bi_2S_3 nanowires can enable highly stable long-term stability. All these results together highlight that PILs-promoted electrocatalysis is possible on a conventionally catalytically inactive material.

In summary, we have introduced PILs as effective additives that enable a remarkable level of control over morphogenesis of Bi_2S_3 crystals, which should also allow the access to controlled and sophisticated structures of other inorganic materials, considering their self-structured features and striking binding ability. The achieved Bi_2S_3 crystals demonstrate tunable E_g, which is most likely due to the quantum size effects. Intriguingly, Bi_2S_3 with appropriate PILs modification was found to catalyze water oxidation efficiently and robustly, although its commercial counterpart is catalytically inert. This promotional effect could be originated from altered surface electronic properties of Bi_2S_3 that create catalytically active sites.

Acknowledgments

This work was supported by the Max Plank Society. M.G. thanks the support from CAS Pioneer Hundred Talents Program. S.Y. thanks the funding support from the National Natural Science Foundation of China (Grant 21431006), the Foundation for Innovative Research Groups of the National Natural Science Foundation of China (Grant 21521001), and the National Basic Research Program of China (Grants 2014CB931800, 2013CB931800). J.Y. thanks the European Research Council Starting Grant (639720-NAPOLI).

Keywords: bismuth sulfide · inorganic crystals · morphogenesis · poly(ionic liquid)s · polymer-controlled crystallization

How to cite: *Angew. Chem. Int. Ed.* **2016**, *55*, 12812–12816
Angew. Chem. **2016**, *128*, 13004–13008

[1] a) M. Chhowalla, H. S. Shin, G. Eda, L. J. Li, K. P. Loh, H. Zhang, *Nat. Chem.* **2013**, *5*, 263–275; b) X. B. Chen, S. S. Mao, *Chem. Rev.* **2007**, *107*, 2891–2959; c) Y. N. Xia, Y. J. Xiong, B. K. Lim, S. E. Skrabalak, *Angew. Chem. Int. Ed.* **2009**, *48*, 60–103; *Angew. Chem.* **2009**, *121*, 62–108; d) Z. X. Fan, H. Zhang, *Chem. Soc. Rev.* **2016**, *45*, 63–82; e) H. Zhang, *ACS Nano* **2015**, *9*, 9451–9469; f) Z. X. Fan, M. Bosman, D. Huang, Y. Yu, K. P. Ong, Y. A. Akimov, L. Wu, B. Li, J. Wu, Y. Huang, Q. Liu, C. E. Png, C. L. Gan, P. D. Yang, H. Zhang, *Nat. Commun.* **2015**, *6*, 7684; g) X. J. Wu, J. Z. Chen, C. L. Tan, Y. H. Zhu, Y. Han, H. Zhang, *Nat. Chem.* **2016**, *8*, 470–475.

[2] a) M. Lazzari, M. A. Lopez-Quintela, *Adv. Mater.* **2003**, *15*, 1583–1594; b) S. F. Chen, J. H. Zhu, J. Jiang, G. B. Cai, S. H. Yu, *Adv. Mater.* **2010**, *22*, 540–545; c) F. C. Meldrum, H. Colfen, *Chem. Rev.* **2008**, *108*, 4332–4432; d) H. Cölfen, A. Markus, *Angew. Chem. Int. Ed.* **2005**, *44*, 5576–5591; *Angew. Chem.* **2005**, *117*, 5714–5730.

[3] a) W. L. Leong, P. S. Lee, A. Lohani, Y. M. Lam, T. Chen, S. Zhang, A. Dodabalapur, S. G. Mhaisalkar, *Adv. Mater.* **2008**, *20*, 2325–2331; b) S. B. Darling, *Prog. Polym. Sci.* **2007**, *32*, 1152–1204.

[4] a) J. Y. Yuan, D. Mecerreyes, M. Antonietti, *Prog. Polym. Sci.* **2013**, *38*, 1009–1036; b) J. Y. Yuan, M. Antonietti, *Polymer* **2011**, *52*, 1469–1482; c) D. Mecerreyes, *Prog. Polym. Sci.* **2011**, *36*, 1629–1648; d) P. Kubisa, *Prog. Polym. Sci.* **2009**, *34*, 1333–1347.

[5] D. E. Lee, H. Koo, I. C. Sun, J. H. Ryu, K. Kim, I. C. Kwon, *Chem. Soc. Rev.* **2012**, *41*, 2656–2672.

[6] a) M. R. Gao, Y. F. Xu, J. Jiang, S. H. Yu, *Chem. Soc. Rev.* **2013**, *42*, 2986–3017; b) M. R. Gao, J. Jiang, G. Qiang, S. H. Yu, *Chalcogenide semiconductor based core/shell nanostructures: synthesis, properties and applications, Vol. 2*, American Scientific Publisher, Valencia, **2011**.

[7] a) R. Suarez, P. K. Nair, P. V. Kamat, *Langmuir* **1998**, *14*, 3236–3241; b) G. Konstantatos, L. Levina, J. Tang, E. H. Sargent, *Nano Lett.* **2008**, *8*, 4002–4006.

[8] P. Boudjouk, M. P. Remington, D. G. Grier, B. R. Jarabek, G. J. McCarthy, *Inorg. Chem.* **1998**, *37*, 3538–3541.

[9] K. Yao, Z. Y. Zhang, X. L. Liang, Q. Chen, L. M. Peng, Y. Yu, *J. Phys. Chem. B* **2006**, *110*, 21408–21411.

[10] L. Cademartiri, F. Scotognella, P. G. O'Brien, B. V. Lotsch, J. Thomson, S. Petrov, N. P. Kherani, G. A. Ozin, *Nano Lett.* **2009**, *9*, 1482–1486.

[11] Y. Wang, Y. Y. Wu, Y. J. Liu, J. Shen, L. Lv, L. B. Li, L. C. Yang, J. F. Zeng, Y. Y. Wang, L. W. Zhang, Z. Li, M. Y. Gao, Z. F. Chai, *Adv. Funct. Mater.* **2016**, *26*, 5335–5344.

[12] a) J. M. Kinsella, R. E. Jimenez, P. P. Karmali, A. M. Rush, V. R. Kotamraju, N. C. Gianneschi, E. Ruoslahti, D. Stupack, M. J. Sailor, *Angew. Chem. Int. Ed.* **2011**, *50*, 12308–12311; *Angew. Chem.* **2011**, *123*, 12516–12519; b) O. Rabin, J. M. Perez, J. Grimm, G. Wojtkiewicz, R. Weissleder, *Nat. Mater.* **2006**, *5*, 118–122.

[13] J. Grigas, E. Talik, V. Lazauskas, *Phys. Status Solidi* **2002**, *232*, 220–230.

[14] a) L. Cademartiri, R. Malakooti, P. G. O'Brien, A. Migliori, S. Petrov, N. P. Kherani, G. A. Ozin, *Angew. Chem.* **2008**, *120*, 3874–3877; b) Z. P. Liu, S. Peng, Q. Xie, Z. K. Hu, Y. Yang, S. Y. Zhang, Y. T. Qian, *Adv. Mater.* **2003**, *15*, 936–940; c) Y. M. Cao, M. Bernechea, A. Maclachlan, V. Zardetto, M. Creatore, S. A. Haque, G. Konstantatos, *Chem. Mater.* **2015**, *27*, 3700–3706; d) C. H. Ye, G. W. Meng, Z. Jiang, Y. H. Wang, G. Z. Wang, L. D. Zhang, *J. Am. Chem. Soc.* **2002**, *124*, 15180–15181; e) H. F. Bao, X. Q. Cui, C. M. Li, Y. Gan, J. Zhang, J. Guo, *J. Phys. Chem. C* **2007**, *111*, 12279–12283; f) J. Tang, A. P. Alivisatos, *Nano Lett.* **2006**, *6*, 2701–2706; g) Y. Y. Zhao, K. T. E. Chua, C. K. Gan, J. Zhang, B. Peng, Z. P. Peng, Q. H. Xiong, *Phys. Rev. B* **2011**, *84*, 205330; h) L. S. Li, N. J. Sun, Y. Y. Huang, Y. Qin, N. N. Zhao, J. N. Gao, M. X. Li, H. H. Zhou, L. M. Qi, *Adv. Funct. Mater.* **2008**, *18*, 1194–1201.

[15] J. Black, E. M. Conwell, L. Seigle, C. W. Spencer, *J. Phys. Chem. Solids* **1957**, *2*, 240–251.

[16] Y. Park, K. J. McDonald, K. S. Choi, *Chem. Soc. Rev.* **2013**, *42*, 2321–2337.

[17] M. R. Gao, M. K. Y. Chan, Y. G. Sun, *Nat. Commun.* **2015**, *6*, 7493.

[18] M. Aresti, M. Saba, R. Piras, D. Marongiu, G. Mula, F. Quochi, A. Mura, C. Cannas, M. Mureddu, A. Ardu, G. Ennas, V. Calzia, A. Mattoni, A. Musinu, G. Bongiovanni, *Adv. Funct. Mater.* **2014**, *24*, 3341–3350.

[19] J. Dupont, J. D. Scholten, *Chem. Soc. Rev.* **2010**, *39*, 1780–1804.

[20] a) H. Tsunoyama, N. Ichikuni, H. Sakurai, T. Tsukuda, *J. Am. Chem. Soc.* **2009**, *131*, 7086–7093; b) J. E. Newton, J. A. Preece, N. V. Rees, S. L. Horswell, *Phys. Chem. Chem. Phys.* **2014**, *16*, 11435–11446; c) G. R. Zhang, B. Q. Xu, *Nanoscale* **2010**, *2*, 2798–2804; d) R. J. Tseng, C. O. Baker, B. Shedd, J. X. Huang, R. B. Kaner, J. Y. Ouyang, Y. Yang, *Appl. Phys. Lett.* **2007**, *90*, 053101; e) L. M. Qiu, L. Z. Zhao, W. S. Yang, J. N. Yao, *Langmuir* **2006**, *22*, 4480–4482; f) M. R. Gao, S. R. Zhang, Y. F. Xu, Y. R. Zheng, J. Jiang, S. H. Yu, *Adv. Funct. Mater.* **2014**, *24*, 916–924.

[21] T. L. Barr, *Modern ESCA: The Principles and Practice of X-Ray Photoelectron Spectroscopy*, CRC, Boca Raton, **1994**.

[22] T. P. Debies, J. W. Rabalais, *Chem. Phys.* **1977**, *20*, 277–283.

[23] a) T. Wu, X. G. Zhou, H. Zhang, X. H. Zhong, *Nano Res.* **2010**, *3*, 379–386; b) X. H. Gao, H. B. Wu, L. X. Zheng, Y. J. Zhong, Y. Hu, X. W. Lou, *Angew. Chem.* **2014**, *126*, 6027–6031; c) G. Manna, R. Bose, N. Pradhan, *Angew. Chem.* **2014**, *126*, 6861–6864.

[24] M. Grätzel, *Nature* **2001**, *414*, 338–344.

[25] M. R. Gao, J. X. Liang, Y. R. Zheng, Y. F. Xu, J. Jiang, Q. Gao, J. Li, S. H. Yu, *Nat. Commun.* **2015**, *6*, 5982.

[26] a) R. Subbaraman, D. Tripkovic, K. C. Chang, D. Strmcnik, A. P. Paulikas, P. Hirunsit, M. Chan, J. Greeley, V. Stamenkovic, N. M. Markovic, *Nat. Mater.* **2012**, *11*, 550–557; b) J. Suntivich, K. J. May, H. A. Gasteiger, J. B. Goodenough, Y. Shao-Horn, *Science* **2011**, *334*, 1383–1385.

Received: July 26, 2016
Published online: September 15, 2016

